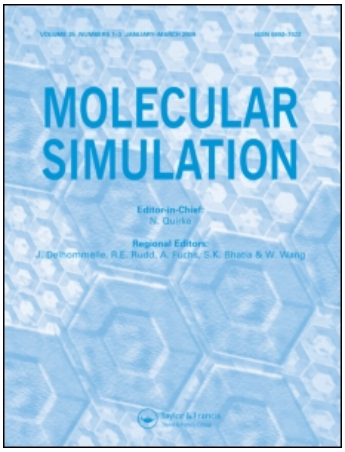

Molecular Simulation
Publication details, including instructions for authors and subscription information:
http://www.informaworld.com/smpp/title~content=t713644482

A Molecular Dynamics Simulation Study of the Density and Temperature Dependence of Self-diffusion in a "Sphere-cylinder" Micropore

T. Demi[a]; D. Nicholson[b]
[a] Institute of Cancer Research, Royal Cancer Hospital, Clifton Avenue, Sutton, Surrey, UK [b] Department of Chemistry, Imperial College of Science, Technology and Medicine, University of London, London, UK

To cite this Article Demi, T. and Nicholson, D.(1991) 'A Molecular Dynamics Simulation Study of the Density and Temperature Dependence of Self-diffusion in a "Sphere-cylinder" Micropore', Molecular Simulation, 7: 1, 121 — 134
To link to this Article: DOI: 10.1080/08927029108022454
URL: http://dx.doi.org/10.1080/08927029108022454

Molecular Simulation, 1991, Vol. 7, pp. 121–134
Reprints available directly from the publisher
Photocopying permitted by license only

A MOLECULAR DYNAMICS SIMULATION STUDY OF THE DENSITY AND TEMPERATURE DEPENDENCE OF SELF-DIFFUSION IN A "SPHERE-CYLINDER" MICROPORE

T. DEMI

Institute of Cancer Research, Royal Cancer Hospital, Clifton Avenue, Sutton, Surrey SM2 5PX, UK

and

D. NICHOLSON*

Department of Chemistry, Imperial College of Science, Technology and Medicine, University of London, London SW7 2AY, UK

(*Received August 1990, accepted September 1990*)

We report Molecular Dynamics calculations of density profiles and self-diffusion coefficients of Lennard-Jones fluids confined in a pore of "sphere-cylinder" geometry consisting of spheres interconnected through cylindrical sections. The geometrical characteristics were the radius of the cylinder $R = 2\sigma$, the ratio of the radius of the cylinder to radius of the sphere $R/R_s = 0.85$ and the ratio of length of cylinder to length of sphere $L/A = 1.5$. The results were compared with previous results on a cylindrical pore of the same radius as that of the cylindrical section of this model and it was found that the self-diffusion coefficients parallel to the pore walls were generally lower although their relative difference was within statistical errors.

KEY WORDS: sphere-cylinder geometry, molecular dynamics, diffusion coefficients.

1 INTRODUCTION

There has been much interest in recent years in understanding the molecular behaviour of particles confined in narrow pores. Many theoretical and computational methods have been used for this purpose. The theoretical studies include density functional theory [1,2,3] and integral equation theory [4]. Most computational studies have been performed on slit [5,6,7] and cylindrical models [8,9,10] using both Molecular Dynamics (MD) and Monte Carlo (MC) computer simulation techniques.

In the present paper we report MD simulations of Lennard-Jones fluids in "sphere-cylindrical" pores in which spheres are interconnected through cylindrical sections. This is as far as we know, the first study in such a model. Geometry of this general type is of interest because it represents, in a very idealized form, the kind of internal structure which is likely to occur in real porous materials; zeolites are one obvious example [10, 11]; networks of spherical sections joined by cylindrical "bonds" are also popular as a means of modelling the less well defined porous materials [12]. The present model is highly simplified in being one dimensional, and because the potential

*Author to whom correspondence should be adressed.

functions do not have any of the complications due to local electrostatic fields which occur in many zeolites, it therefore emphasizes the essential geometric effects on diffusion associated with constricted structures. The geometrical characteristics of the model are: radius of the cylindrical section of the model $R = 2\sigma$, ratio of the radius of the cylinder/radius of the sphere (window opening) $R/R_s = 0.85$ and ratio of the length of the cylinder/length of sphere, $L/A = 1.5$. These were chosen as a first step towards an extensive investigation of the ratio of the radius of cylinder/radius of sphere and of the ratio of the length of cylinder/length of sphere on the self-diffusion coefficients parallel to the pore axis.

2 METHOD

The system was similar to the one reported in [13]; the fluid–fluid interactions were modelled by a Lennard-Jones potential with krypton parameters $\sigma = 0.357\,\text{nm}$ and $\varepsilon/k = 201.9\,\text{K}$, and the fluid--solid interactions were approximated by an average over the uniformly distributed atoms in the solid

$$u_{1s}(\mathbf{r}_i) = \rho_s \int_s u_{ij}(\mathbf{r}_i, \mathbf{r}_j)\, d\mathbf{r}_j$$

where ρ_s is the solid density and $u_{ij}(\mathbf{r}_i, \mathbf{r}_j)$ is the Lennard-Jones potential. The energy parameter $\rho_s\varepsilon_{1s}/K = 1315\,\text{knm}^{-2}$ and $\sigma_{1s} = 0.3165\,\text{nm}$. The "sphero-cylindrical" geometry [Figure 1] consisted of spheres of radius R_s measured from the centre of the pore to the centre of the wall atom and length A, interconnected through cylindrical sections of radius R and length L. The radius of the cylindrical section of the model was kept the same as in the cylindrical geometry already investigated [13], that is $R = 2\sigma$, in order to facilitate comparison of diffusion results. The ratio of the radius of the cylinder/radius of sphere, $W = R/R_s$, was 0.85 and the effective value $W' = (R - 0.5)/(R_s - 0.5)$ was 0.81; the ratio of length of cylinder/length of sphere L/A was 1.5. These geometrical parameters correspond to a 20% or 25% increase in volume (with or without taking into account the volume excluded by the dimensions of the wall atoms respectively), compared to a totally cylindrical model. A two-dimensional rectangular grid in the z and t-directions (parallel and perpendicular to the pore walls) was created for the potential energy and force calculations in t and z-directions (see Figure 1). The number of the tabulated points was 65 for both directions. No calculations were performed at points lying outside the pore. A bi-linear interpolation method was used to interpolate between tabulated points. Unfortunately the method was found to be numerically inaccurate in some of the grid squares, especially close to the pore walls and the following method was developed to trap these problematic squares. The potential energy and forces were first calculated at the middle point of each grid square. The values were then compared with the interpolated ones at the same point and the relative errors were recorded in a separate file. If, during the course of the simulation, a point lies within a grid square where the relative error was greater than the required value, calculation instead of interpolation was performed. The required relative error for the present simulations was chosen to be 1×10^{-3}. The numerical equations of motion were solved using Verlet's Leap Frog algorithm [14,15] with a time step of 2.5×10^{-3} ps. Periodic boundary conditions were employed only in the z direction (taken along the pore axis). The starting configuration was formed by placing annular monolayers of atoms perpendicular to the axis of a cylinder of the

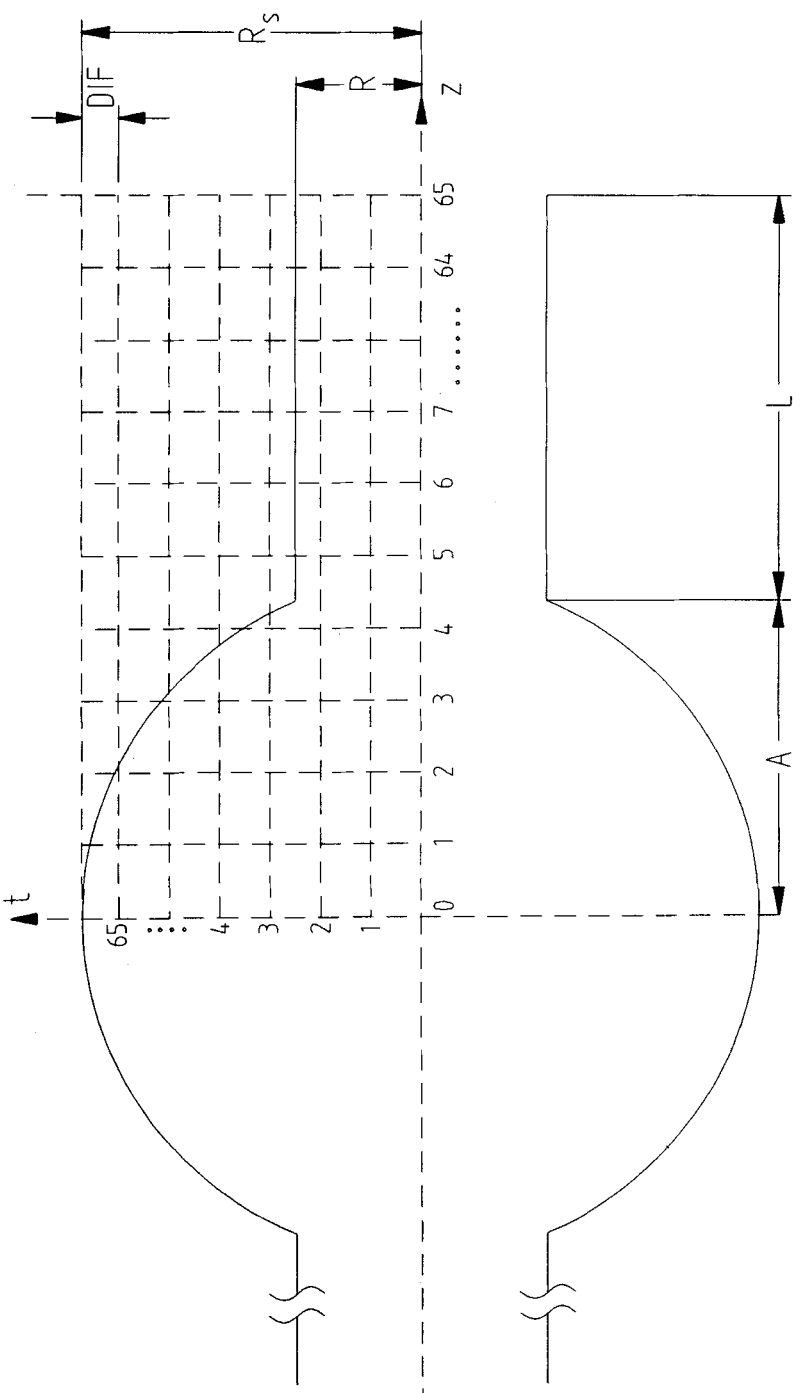

Figure 1 Model of a "sphere-cylinder" geometry. R_s: radius of the sphere, R: radius of cylinder, A: length of sphere, L: length of cylinder. The broken lines show the two-dimensional interpolation grid. The number of rows and columns were both set to 65.

same radius as that of the cylindrical section of the model, that is $R = 2\sigma$ and of the same length as that of the MD simulation box. The overall density of the system was calculated by taking into account the dimensions of the wall atoms. The initial velocities of the particles were chosen from a Maxwell-Boltzmann distribution. The number of the production time steps of the simulation was between 10000–30000 depending on the temperature and density of the system. A post-simulation method developed earlier [16] was used for the calculation of the MSD and VACF. The simulations were performed on the CRAY X/MP at the University of London Computer Centre.

3 RESULTS AND DISCUSSION

3.1 Density Profiles

Radial density profiles were produced by dividing half the central cavity of the MD box into 8 z-slices, 4 dividing the spherical and another 4 the cylindrical section of the model. The radius of each z-slice lying in the spherical part of the model was the average of its maximum and minimum radius. On the other hand the radius of the slices lying in the cylindrical part was $R = 2\sigma$. The length of the first 4 slices was $A/4$ and of the other 4, $L/4$. The density was calculated in each bin by counting the number of particles in the bin averaged over all cavities of the MD box, and dividing by the volume of the bin.

$$\rho_{r_i} = \frac{\langle N_i \rangle}{\pi \left[(\mathbf{r}_i + \Delta\mathbf{r}/2)^2 - (\mathbf{r}_i - \Delta\mathbf{r}/2)^2\right] \Delta z_i}$$

where $\mathbf{r}_i$ denotes the radial coordinates of the centre of the ith bin, and z_i is the axial length of the bin. The $\langle \ldots \rangle$ in the numerator indicates a time average of N_i, the number of particles in the ith bin. Figures 2 and 3 present local density profiles in different z-slices, at $n_p \sigma^3 = 0.82$ and $kT/\varepsilon = 1.49$ and 2.98 respectively. Also Figures 4 and 5 show local density profiles in different slices at $n_p \sigma^3 = 0.4$ and $kT/\varepsilon = 1.49$ and 2.98 respectively. The importance of packing effects in dense fluids [17] is clearly shown in these figures. At $kT/\varepsilon = 1.49$ and 2.98 and at the higher mean density two peaks at radial distance of 0.5σ and 1.5σ from the centre of the pore were observed in the density profile of the slice closest to the centre of the spherical cavity (mean radius $R_m = 2.34\sigma$). As R_m of the subsequent slices decreases the first peak flattens and moves towards the axial region. Also due to this decrease in the mean radius, the peak at the wall is shifted away from the pore walls. In all these figures, the density profile of the slice closest to the beginning of the cylindrical section is quite similar in appearance to those within the cylindrical section. This suggests that the large window opening ($W = 0.85$) has little influence on the density distribution in the region near to the beginning of the cylindrical section. The density profiles in the cylindrical part are very similar to those already found in the corresponding cylindrical model [13].

3.2 Self-Diffusion Coefficients

In equilibrium MD simulations self-diffusion coefficients parallel and perpendicular to the pore walls can be calculated by the numerical integration of the velocity auto-correlation function (VACF) and by the slope of the mean square-displacement

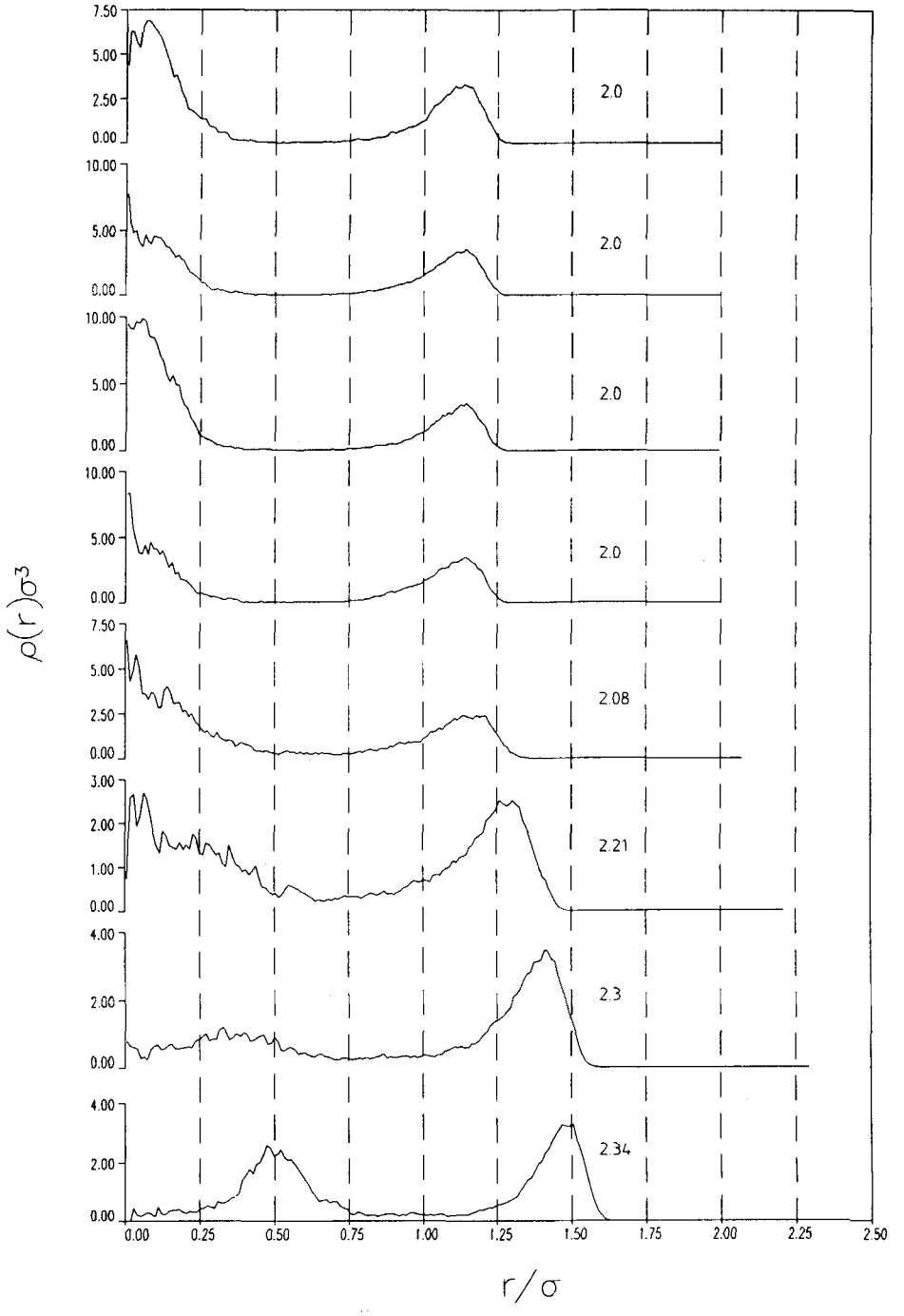

Figure 2 Density profiles for different z-slices obtained from MD data. The temperature is $kT/\varepsilon = 1.49$ and density $n_p \sigma^3 = 0.82$. Starting at the bottom of these figures the first 4 graphs show the local density profiles in the slices dividing the spherical part of the model, while the next 4 show local density profiles in the cylindrical part. The number on the right of the peak at the wall indicates the mean radius for each z-slice. Note that the scale on the y-axis is not the same for all graphs.

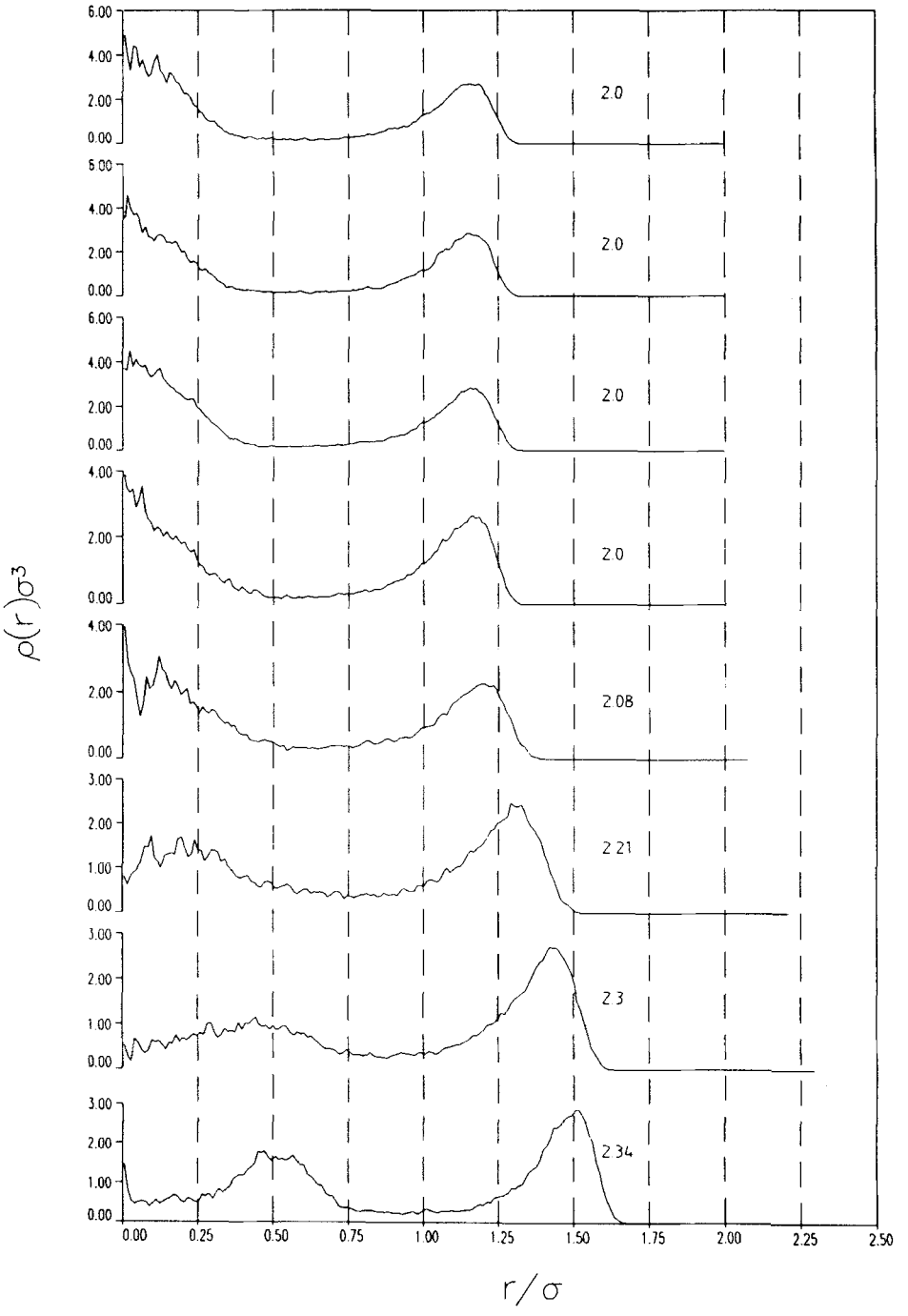

Figure 3 Density profiles, as in Figure 2 with $kT/\sigma = 2.98$, $n_p \sigma^3 = 0.82$.

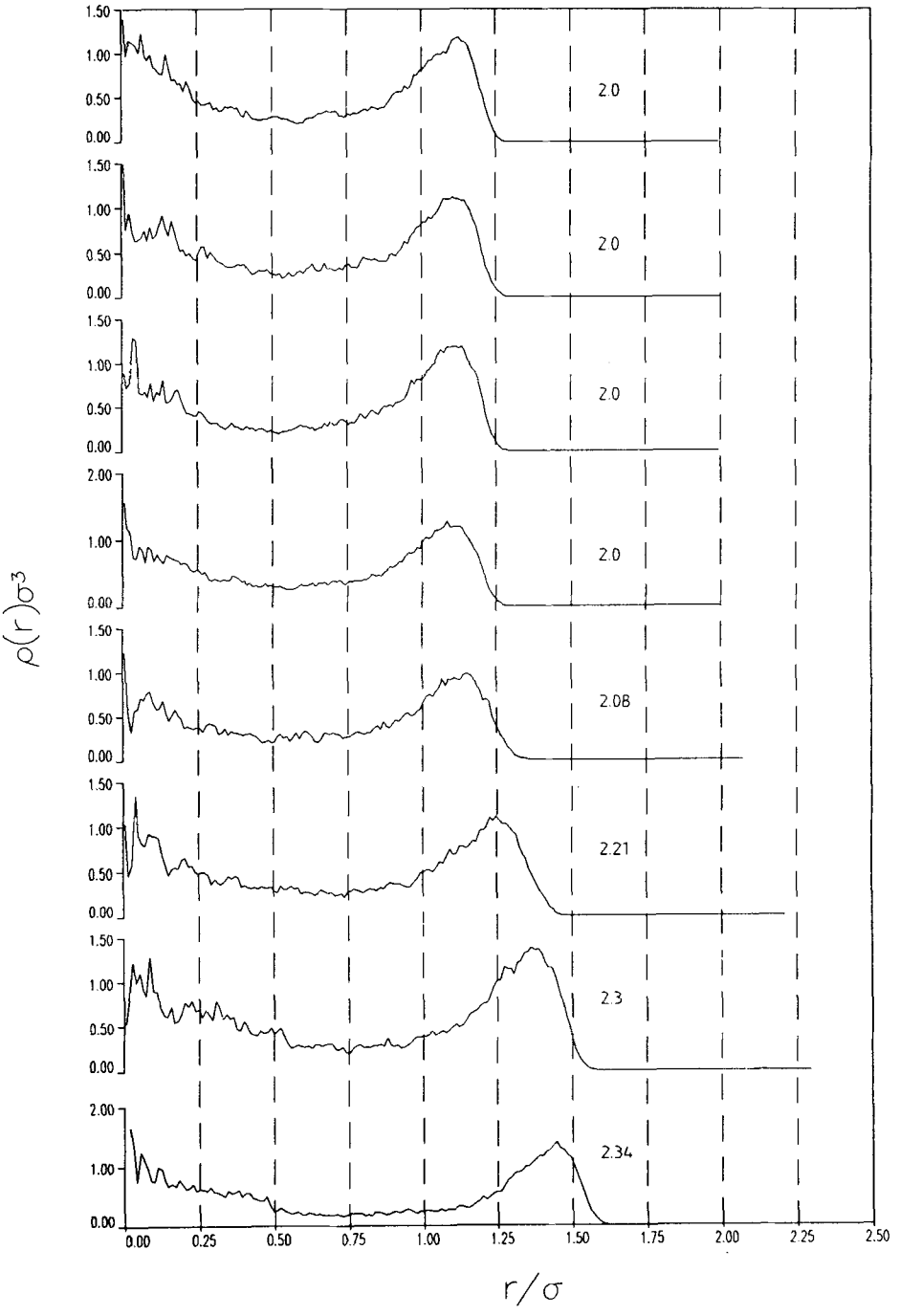

Figure 4 Density profiles as in Figure 2 with $kT/\varepsilon = 1.49$, $n_p \sigma^3 = 0.4$.

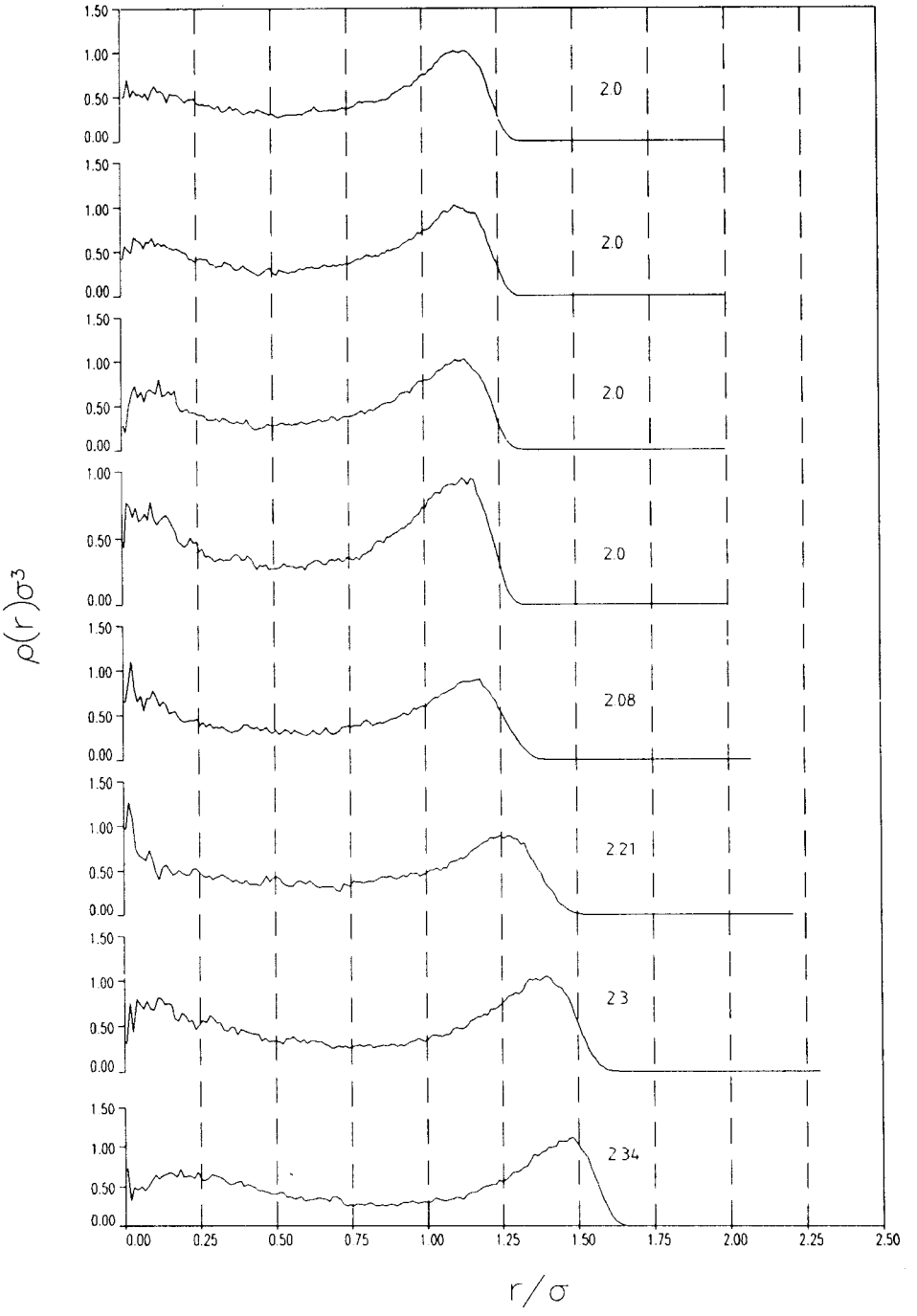

Figure 5 Density profiles as in Figure 2 with $kT/\varepsilon = 2.98$, $n_p \sigma^3 = 0.4$.

Table 1 $D_{\|}^{*}$ from MSD data at different temperatures in a cylindrical and "sphere-cylinder" model. The density is $n_p \sigma^3 = 0.82$. The last column presents the bulk value [18].

kT/ε	$D_{\|}^{*}$ (cyl)	$D_{\|}^{*}$ (sph-cyl)	D_b^{*}
0.49	0.025	0.026	0.015
1.49	0.109	0.096	0.099
2.98	0.218	0.196	0.202

(MSD) vs. time. In the former, the self-diffusion coefficient is given by

$$D_{\|} = \int_0^{\infty} \left[(1/N) \sum_{i=1}^{N} \langle v_{1z}(t)\, v_{1z}(0) \rangle \right]$$

here v_i denotes the vth component of the velocity of particle i at time t, and N is the number of the particles in the simulation box, $\langle ... \rangle$ indicate that the quantity $(v(t)_{iv}$ $v(0)_{iv})$ is averaged over all particles in the simulation box and over a number of time origins. From the mean square displacement (MSD)

$$D_{\|} = \lim_{t \to \infty} (1/N) \left[\sum_{i=1}^{N} (1/2t) (\langle Z_i(t) - Z_i(0))^2 \rangle) \right]$$

where $Z_i(t)$, $Z_i(0)$ are the components of the position vectors of particle i at time t and time origin 0 respectively.

3.2.1 Temperature and density dependence

The temperature dependence of $D^{*}_{\|}$ has been studied at two densities $n_p \sigma^3 = 0.82$ and 0.4 and at a series of temperatures. The results were compared with previously reported results for a cylindrical geometry. In Tables 1 and 2 we present the values of $D_{\|}^{*}$ in both the cylindrical and "sphere-cylinder" models and the bulk value D_b^{*} calculated from [18], at the two densities respectively and for a series of temperatures. Figures 6 and 7 show the temperature dependence of the self-diffusion coefficients in the two models and in the bulk. There is a general trend for $D_{\|}^{*}$ to be lower than in the cylindrical model in both figures, although the relative difference is within statistical errors. This result is consistent with a previously reported observation [16] that $D_{\|}^{*}$ remains approximately the same when the radius of a cylindrical pore increases from 2 to 5σ. At the lower density and $kT/\varepsilon > = 0.8$ (Figure 7), $D_{\|}^{*}$ is consistently lower than the corresponding values in the cylindrical model and in the bulk although that may well be the result of an artifact of the simulations (the number of time origins in

Table 2 Same as Table 1 but for $n_p \sigma^3 = 0.4$

kT/ε	$D_{\|}^{*}$ (cyl)	$D_{\|}^{*}$ (sph-cyl)	D_b^{*}
0.49	0.044	0.050	0.108
0.62	0.094	0.088	0.166
0.74	0.213	0.231	0.212
0.99	0.328	0.323	0.295
0.86	0.296	0.244	0.257
1.49	0.452	0.370	0.429
2.98	0.748	0.630	0.793

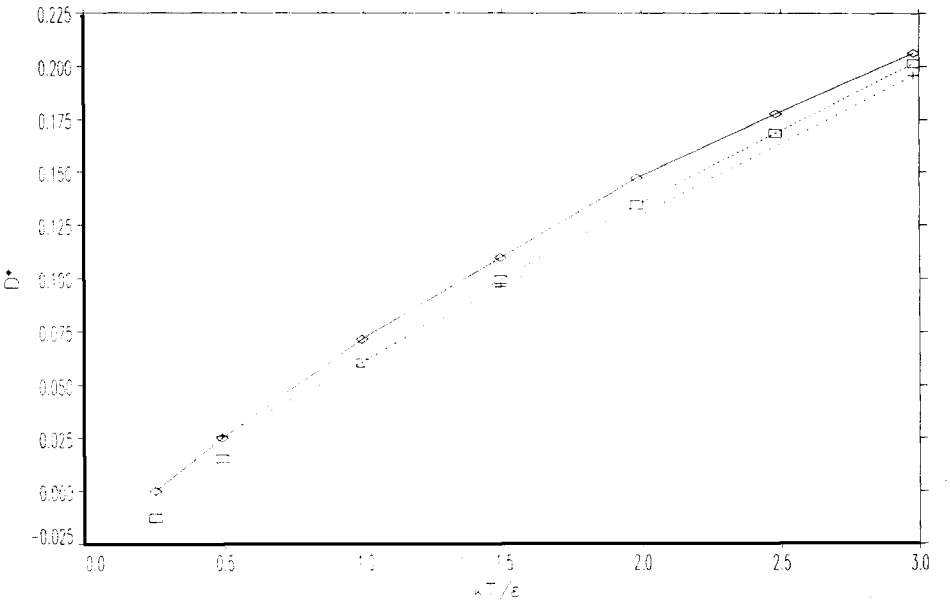

Figure 6 Self-diffusion coefficients parallel to the pore walls, $D_{\parallel}^{*}$ in a cylindrical (□) and "sphere-cylinder" model (+) as a function of temperature. Also shown in the bulk value (◇) calculated from [18]. The density is $n_p \sigma^3 = 0.82$.

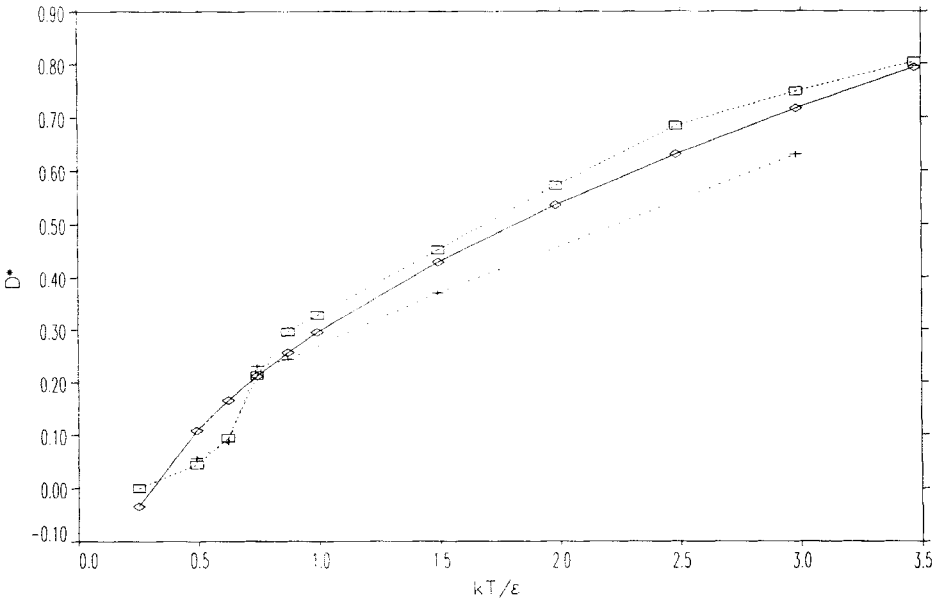

Figure 7 Same as Figure 6 but at $n_p \sigma^3 = 0.4$.

Table 3 $D_{\parallel}^{*}$ calculated from MSD data at different densities in a cylindrical and "sphere-cylinder" model. The last column presents the bulk value calculated from [18]. The temperature is $kT/\varepsilon = 1.49$.

$n_p\sigma^3$	$D_{\parallel}^{*}$ *(cyl)*	$D_{\parallel}^{*}$ *(sph-cyl)*	D_b^{*}
0.20	0.893	0.818	1.010
0.40	0.452	0.370	0.429
0.82	0.109	0.096	0.099

the simulations in a "sphere-cylinder" model was in the range 5000–10000 while the ones in a cylindrical model were in the range 10000–20000). Table 3 presents the calculated values of $D_{\parallel}^{*}$ in both models and in the bulk [18] at $kT/\varepsilon = 1.49$ and a series of densities. Figure 8 shows the density dependence of $D_{\parallel}^{*}$ in the two models and in the bulk. Again the relative difference of the values in the two models is within the statistical errors. Larger deviations are observed only at low densities of $n_p\sigma^3 <= 0.4$. This may be due to the inaccurate calculation of self-diffusion coefficients from MSD and/or VACF simulation data at these low densities (large negative long time tail in VACF [13]).

The behaviour of the $MSD_{\perp}$ and $VACF_{\perp}$ perpendicular to the pore walls at the finite time of 4.5ps is also worth mentioning. At $kT/\varepsilon = 0.5$ and $n_p\sigma^3 = 0.82$ and 0.4 the break of the slope of the $MSD_{\perp}$ vs. time appears at approximately the same time as that in a totally cylindrical model but it is less severe at both densities (Figure 9). The negative backscattering minimum in the corresponding VACF's is smaller as well (Figure 10). No such behaviour is observed at $kT/\varepsilon = 2.98$ because the break in the

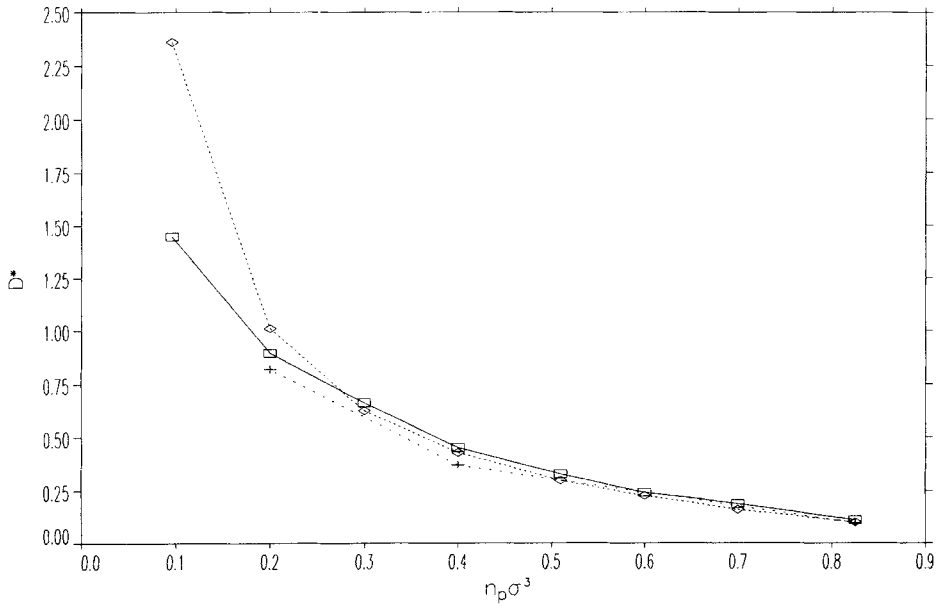

Figure 8 Self-diffusion coefficients parallel to the pore walls $D_{\parallel}^{*}$ in a cylindrical (□) and a "sphere-cylinder" (+) model as a function of density. Also presented is the bult value (◇) calculated from [18]. The temperature is $kT/\varepsilon = 1.49$.

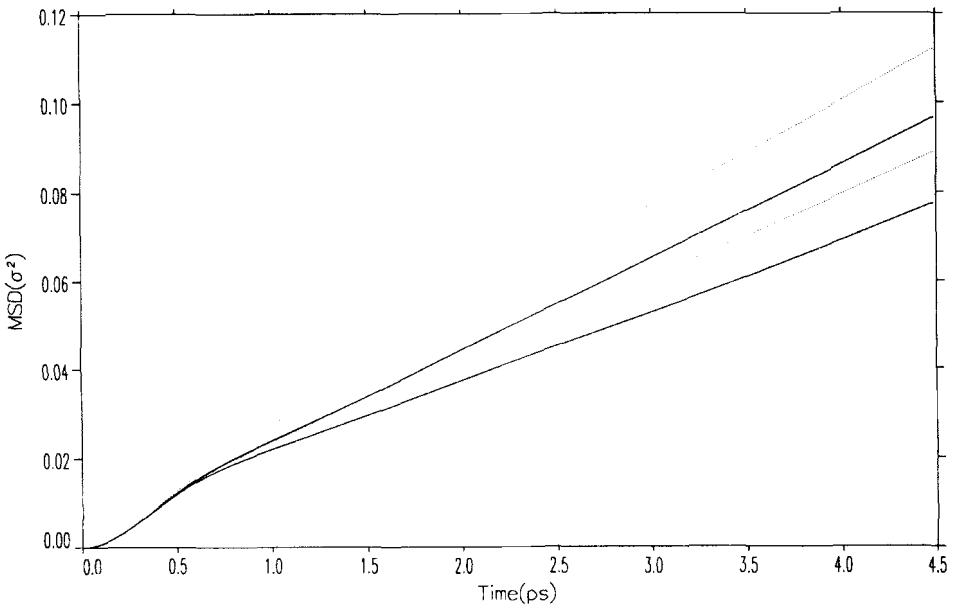

Figure 9 MSD perpendicular to the pore walls for the cylinder (solid lines) and "sphere-cylinder" (dotted lines) models at densities 0.82 (upper two graphs) and 0.4 (lower two graphs) and temperature $kT/\varepsilon = 0.5$.

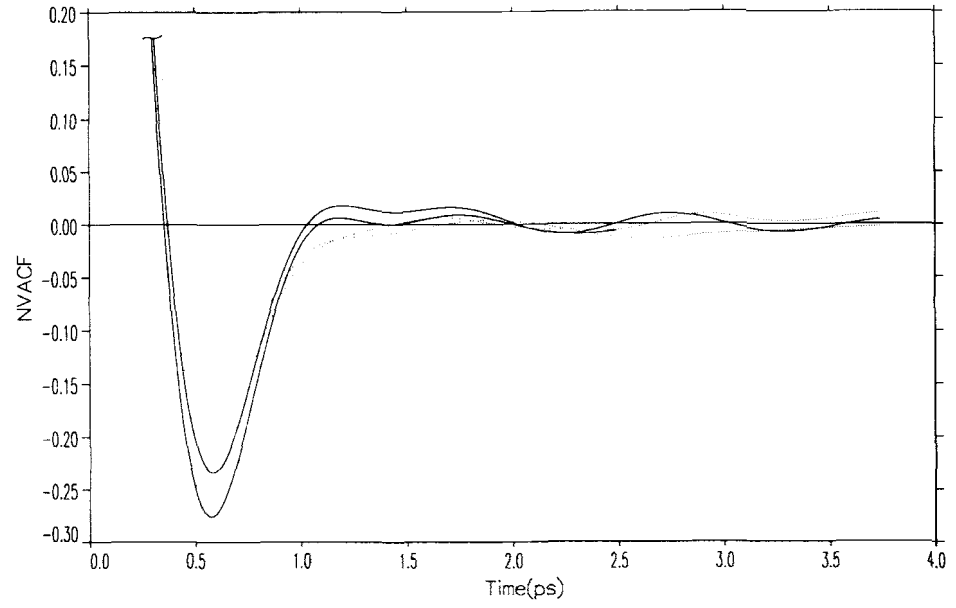

Figure 10 VACF perpendicular to the pore walls in the cylinder (solid curves) and "sphere-cylinder" (dotted curves) models at densities 0.82 (graphs with the deepest minimum in each model) and 0.4 (graphs with the shallowest minimum in each model). The temperature is $kT/\varepsilon = 0.5$.

slope of the $MSD_\perp$'s is absent at these high temperatures. The soundwave hypothesis [7] has already been given as an explanation of the break of the slope of the $MSD_\perp$ vs. time. The fact that the break in the slope is less severe in the "sphere-cylinder" model suggests that the spherical section of the model reduces the backscattering of the particles due to the developed sound waves.

3.3 Conclusions

We have presented density profiles and self-diffusion coefficients in a "sphere-cylinder" model, in which spheres are interconnected through cylindrical sections, for various temperature and densities. The geometrical parameters were: radius of cylinder $R = 2\sigma$, ratio of radius of cylinder/radius of sphere $R/R_s = 0.85$ and ratio of length of cylinder/length of sphere $L/A = 1.5$. This corresponds to a 20% increase in cavity volume compared to a totally cylindrical model. The self-diffusion coefficients parallel to the pore walls were found to be the same as those in the corresponding cylindrical model within statistical error. In the near future we intend to investigate the effect of the length of cylinder/length of sphere and also of the window opening (radius of cylinder/radius of sphere) on self-diffusion.

Acknowledgments

We wish to thank Mr. S. Bleazard for his help with computing and Dr. N. Parsonage for helpful discussions. Many thanks to the British Council for a maintenance grant (to TD) and the University of London Computer Centre for a generous allocation of computer time.

References

[1] R. Evans, U. Marini Bettolo Marconi and P. Tarazona. Fluids in narrow pores: Adsorption, capillary condensation, and critical points. *J. Chem. Phys.*, **84**, 2376.
[2] R. Evans, U. Marini Bettolo Marconi and P. Tarazona. *J. Chem. Soc. Faraday Trans.* II, **82**, 1763.
[3] B.K. Peterson, J.P.R.B. Walton and K.E. Gubbins. Fluid behaviour in narrow pores. *J. Chem. Soc. Faraday Trans* II, **82**, 1789.
[4] U. Heinbuch and J. Fischer. Liquid argon in a cylindrical carbon pore: Molecular Dynamics and Born-Green-Yvon results. *Chem. Phys. Let.*, **135** (6), 587–590, (1987)
[5] V.Ya. Aantonchenko, V.V. Ilyin, N.N. Makovsky, A.N. Pavlov and V.P. Sokhan. On the nature of disjoining pressure oscillations in fluid films. *Molecular Physics*, **52** (2), 345–355, (1984).
[6] S. Subramanian and H.T. Davis. Molecular Dynamics of a hard sphere fluid in small pores. *Molecular Physics* **38** (4), 1061–1066, (1979).
[7] J.J. Magda, M. Tirrell and H.T. Davis. Molecular Dynamics of liquid-filled pores. *J. Chem. Phys.*, **83a**(4), 1888–1895, (1985).
[8] L.B.K. Peterson and K.E. Gubbins. Phase transitions in a cylindrical pore. Grand Canonical Monte Carlo, Mean Field theory and the Kelvin equation. *Molecular Physics*, **62** (1), 215–226, (1987).
[9] S.H. Suh and J.M.D. MacElroy. Molecular Dynamics simulation of hindered diffusion in microcapillaries. *Molecular Physics*, **58** (3), 445–473, (1986).
[10] G.B. Woods, A.Z. Panagiotopoulos and J.S. Rowlinson. Adsorption of fluids in model zeolite cavities. *Molecular Physics*, **63** (1), 49–63, (1988).
[11] N. Kanellopoulos, K.A. Munday and D. Nicholson. The flow of a non-adsorbed, collisionless gas through linked spheres. A model for zeolite diffusion. *J Membrane Science*, **13**, 247–258, (1983).
[12] G. Mason. A model of adsorption-desorption hysteresis in which hysteresis is primarily developed by the interconnection in a network of pores. *Proc. Roy. Soc.*, **A390**, 47–72 (1983).
[13] T. Demi and D. Nicholson. Molecular dynamics simulation studies of the density and temperature dependence of self-diffusion in a cylindrical micropore. *Molecular Simulation*, **5**, 363–381 (1991).

[14] R.W. Hockney. The potential calculation and some applications. *Methods Comput. Phys.*, **9**, 136–211, (1956).
[15] D. Potter. *Computational Physics*, Wiley, New York, (1972).
[16] T. Demi. PhD thesis, University of London, (1989).
[17] McSchoen, D.J. Diestler and J.H. Cushman. Fluids in micropores. I. Structure of a simple classical fluid in a slit pore. *J. Chem. Phys.* **87**, 5464–5470 (1987).
[18] D.M. Heyes. Self-diffusion and shear viscosity of simple fluids. *J. Chem. Faraday Trans. 2*, **79**: 1741–1747, (1983).